Reg 7334 Copy 213

[redacted] CONFIDENTIAL

RM A55E17

NACA RM A55E17

6452

NACA

RESEARCH MEMORANDUM

LOAD DISTRIBUTIONS ON WINGS AND WING-BODY COMBINATIONS AT HIGH ANGLES OF ATTACK AND SUPERSONIC SPEEDS

By Elliott D. Katzen and William C. Pitts

Ames Aeronautical Laboratory
Moffett Field, Calif.

Classification cancelled (or changed to UNCLASSIFIED)

By Authority of NASA Tech Pub Announcement #39
(OFFICER AUTHORIZED TO CHANGE)

By .... 16 FEB 61

WAB
GRADE OF OFFICER MAKING CHANGE)

14 MARCH 61
DATE

NATIONAL ADVISORY COMMITTEE FOR AERONAUTICS

WASHINGTON

July 21, 1955

CONFIDENTIAL [redacted]

 [redacted]

NATIONAL ADVISORY COMMITTEE FOR AERONAUTICS

RESEARCH MEMORANDUM

LOAD DISTRIBUTIONS ON WINGS AND WING-BODY COMBINATIONS AT HIGH ANGLES OF ATTACK AND SUPERSONIC SPEEDS

By Elliott D. Katzen and William C. Pitts

INTRODUCTION

Maximum loads on present-day airplanes have generally been reached at high speed and high dynamic pressures at relatively low altitudes and low angles of attack. For aircraft which are required to maneuver rapidly at extreme altitudes, maximum loads are reached at high angles of attack. For the Mach numbers considered in present designs, loads information is necessary for both flight conditions. To provide the required information, extensive research programs have been undertaken (ref. 1, 2, and 3). In figure 1, the scope of the investigations is outlined. Data were obtained through the Mach number range from 1.45 to 3.36, which covers the current range in design for airplanes and missiles. The angle-of-attack range of the tests was 0° to 45°. The wing sweepback angles varied from 0° to 85°. In addition to wings alone, wing-body combinations were also studied.

The data obtained illustrate many nonlinear effects which make accurate prediction of loads difficult. These nonlinear effects on loads are usually, but not always, alleviating. They occur at low, as well as at high, angles of attack. The purpose of the present paper is to summarize these nonlinear effects and to indicate where departures from linearity and linear-theory predictions become important.

RESULTS AND DISCUSSION

Wings

Departures from the predictions of linear theory, for a thin wing, depend on sweep angle, Mach number, and angle of attack. For moderate sweep, moderate supersonic Mach numbers, and low angles of attack, linear theory is expected to give adequate answers. An example of such a case will be presented; then, typical nonlinear effects of variations in these test parameters will be illustrated.

An example of a case in which linear theory is applicable is shown in figure 2. The delta wing has an aspect ratio of 4, corresponding to

[redacted]

[redacted]

a sweepback angle of 45°. The wing section is 5-percent thick and has a trailing edge of 50-percent bluntness. The Mach number is 1.45 and the Reynolds number, based on the wing mean aerodynamic chord, is 2.1×10^6. At 3° angle of attack it is seen that agreement between theory and experiment is good. It is best at the inboard stations, toward the leading edge, and deteriorates somewhat toward the trailing edge and at the outboard stations. Curiously, even at 20° angle of attack where linear theory is not expected to be applicable, the agreement is still good at the inboard stations. At the 75-percent-semispan station the effects of separation and shock waves on the wing are large and are not accounted for theoretically. The predicted tip loads are higher than the experimental values so that wing bending moments, predicted on the basis of linear theory, would be conservative.

As the wing aspect ratio is reduced, or the leading-edge sweep increased, viscosity and separation affect a larger part of the wing. These results are exemplified (fig. 3) by a delta wing having a very low aspect ratio. The wing semiapex angle is 5°, corresponding to an aspect ratio of about 1/3. The wing section is a 1-percent-thick wedge with a trailing edge of 100-percent bluntness. The Mach number is 1.9 and the Reynolds number, based on the mean aerodynamic chord, is about 1×10^7. In figure 3, upper- and lower-surface lifting pressures are presented for the local semispan at the 78-percent-root-chord station. In addition to the experimental data at 3° and 6° angle of attack, linear theory is shown, and also a vortex theory (ref. 4) developed by Brown and Michael. The vortex-theory curve pertains to 3° angle of attack. The theory was developed by using a vortex model as shown, except that, for simplicity in the calculations, the spiral sheet was replaced by a concentrated vortex and a flat feeding sheet of vorticity. On the upper surface, at 3° angle of attack, the experimental data exhibit a region of increased suction, compared to linear theory, at about 75 percent of the semispan. The increased suction causes the total wing load, as predicted by linear theory, to be too low, or unconservative. At 6° angle of attack the suction peak moves inboard. The vortex theory also shows a suction peak at 3° but the magnitude and position are not properly estimated. The theory does predict inboard movement of the suction peak with increased angle of attack. Thus, qualitatively but not quantitatively, the estimated effects are in agreement with the experimental results for this wing which has a very low aspect ratio. For quantitative prediction, it appears that the simple vortex model must be modified.

As the Mach number and aspect ratio are increased the important nonlinear effects are no longer caused by viscosity and separation. Instead, there are nonlinearities from compression and expansion. An example of these effects is shown in figure 4. The Mach number is increased to 3.36 and the aspect ratio to 4. The wing is the same as that for which data were presented in figure 2 for a Mach number of 1.45. The section is 5-percent thick and has a trailing edge of 50-percent bluntness. The

Reynolds number is 2.1×10^6. The lifting-pressure coefficients are plotted along the chord for the various spanwise stations. The linear theory indicates uniform loading for that part of the wing forward of the Mach wave from the apex, with decreased loading behind the Mach wave. Comparison of the experimental data and linear theory shows large systematic differences, even at 3° angle of attack. The predicted loading is too low at the leading edge and too high at the trailing edge, so that the wing torsional loads would not be estimated properly.

For that part of the wing forward of the influence of the apex, a nonlinear solution can be obtained by extension of the shock-expansion method to three dimensions. This has been done by Vincenti and Fisher at the Ames Aeronautical Laboratory (ref. 5). In figure 5, theoretical curves obtained by this method for the wing at 0° and 3° angle of attack are shown. Linear theory, and the experimental data for that part of the wing forward of the influence of the apex, are also shown. The surface-pressure coefficients (due to wing thickness) at 0° and the lifting pressures at 3° are presented as functions of percentage distance along the local chord. The experimental data from the various spanwise stations have, at given chordwise positions, approximately the same value of surface-pressure and lifting-pressure coefficients. This means that the flow is essentially conical with respect to the tip; that is, the pressures are constant along rays from this point. This is to be expected, as the wing is a cone with respect to the tip; the geometry can be described by directions from this point since there is no characteristic length in the problem. For the pressures due to wing thickness at 0° angle of attack the differences between the linear theory and the three-dimensional shock-expansion theory are not large and there is good agreement with experiment. For the lifting pressures at 3° angle of attack, however, it is seen that the variation of lifting pressure along the chord is estimated more accurately by the three-dimensional shock-expansion theory. This theory is applicable to shock detachment, which occurs at about 15° angle of attack for this wing and Mach number. The differences between pressures given by three-dimensional shock-expansion theory and those predicted by the more familiar two-dimensional theory, for streamwise sections, are small for the present case. For example, at 10° angle of attack, the largest differences (10 percent to 15 percent) occur on the lower surface. On the upper surface the differences between the two theories are negligible at this Mach number of 3.36. For lower Mach numbers or more highly swept wings, the differences are larger. The differences are decreased as the Mach number normal to the leading edge is increased.

The nonlinearity in load distribution between the upper and lower surfaces of the wing at a Mach number of 3.36 and at high angles of attack is illustrated in figure 6. The wing is at 20° angle of attack where the bow wave is detached from the leading edge of the wing. At this angle of attack, the upper-surface pressure coefficients are approaching a vacuum. The variation in lower-surface pressures along the chord resembles that given by two-dimensional shock-expansion theory, for streamwise sections, or Newtonian theory; but, as would be expected, the magnitudes are not given properly. As the angle of attack is increased beyond 20°, the upper-surface pressures approach a vacuum more closely. At 45° angle of attack, a 90-percent vacuum was reached.

Wing-Body Combinations

For the wing-body combinations, there are additional nonlinear effects resulting from interference. These nonlinearities are evaluated by comparison of high-angle experimental data with low-angle data or with existing slender-body or linear theories (ref. 6). For example, the result of body interference on wing-load distribution at angles of attack is shown in figure 7. The wing is the same aspect-ratio-4 wing studied previously. The ratio of body radius to wing semispan is 0.2 and the Mach number is 3.36. The nondimensional span loading, as a function of the percentage distance along the wing semispan, is given for 6° and 20° angle of attack. The normal-force coefficients, from the integrated span loadings, are shown for the angle-of-attack range. At 6° angle of attack, the loading for the wing in the presence of the body is increased by the body upwash over that for the wing alone. It would be unconservative to estimate the loads on the wing of the combination by using wing-alone data and ignoring the interference. The integrated increase in loading on the wing, as shown by the normal-force coefficient, is given accurately at 6° by the theory. At 20° angle of attack, however, the loading of the wing in the presence of the body is only slightly increased over that of the wing alone. This is also the case for the normal-force coefficient above about 10° angle of attack. The estimated wing bending moments would be conservative if the slender-body interference factor were used at high angles of attack.

The results of the interference of the body on wing-load distribution at angles of incidence - that is, incidence relative to the body - are illustrated in figure 8. Nondimensional span loading with the wing at 6° and 20° incidence and the body at 0° angle of attack is shown and the normal-force coefficients for the incidence angles from 0° to 40° are also presented. The span loadings for the wing alone are not greatly different from those of the wing in the presence of the body. The interference (the difference between the span loading for the wing alone and that for the wing of the combination) is less at 6° incidence than at 6° angle of attack. This is especially so for the span loading on the outboard part of the wing. Near the root, at 6° and 20° incidence angles, the loading on the wing of the combination is reduced from that of the wing alone because the body is not a perfect reflection plane, due to its curvature. The normal force on the wing of the combination is predicted with good accuracy throughout the incidence range from 0° to 40° by applying a small interference factor from slender-body theory (ref. 6) to the experimental wing-alone results.

The effect of the presence of the wing on body loading at angles of attack is shown in figure 9. The local body loading along the body length at 6° and 20° angle of attack and the normal-force coefficients as a function of angle of attack are presented. At both angles of attack the loading on the afterbody of the body alone is given with fair accuracy by the viscous-crossflow method (see, for example, ref. 7). At 6° angle of attack the loading carried over from the wing is increased in the region near the wing and decreases toward the base of the body. At 20° angle of attack the presence of the wing is felt forward of the wing through the boundary layer on the body. In this forward region the loading starts to increase slightly. Near the wing the loading is increased rapidly. Behind the wing, the interference loading over the afterbody does not decrease toward the body base. This is a different result than at 6° angle of attack, or at high angles of attack at lower supersonic Mach numbers (see, for example, ref. 8). The integrated increase in normal force on the body, due to the wing, is predicted with good accuracy at high angles of attack even though the bending moments on the rear of the body, predicted by extrapolating from low-angle pressure data, would be unconservative.

The interference load distribution on the body with the wing at angles of incidence is illustrated in figure 10. The body is at 0° angle of attack so that the loading on the body alone is zero. The local loading along the body length for the body in the presence of the wing at 6° and 20° incidence angles and the normal-force coefficients of the body as a function of incidence angles from 0° to 40° are presented. At 6° incidence the loading on the body increases in the region of the wing and decreases toward the base in much the same manner as the loading at an angle of attack. At 20° incidence, however, the positive pressures from the lower surface of the wing are felt on the top of the body near the raised, or unported, wing leading edge. The result is a downward, or negative, loading on the body. Further downstream, the body loading becomes positive, decreasing toward the base of the body. The bending moments on the body at high angles of wing incidence could not be predicted by extrapolating low-angle data.

The effect on the agreement between theory and experiment of the negative loading is also shown for normal-force coefficients. At low incidence angles, the predicted normal force is in good agreement with experiment. Above about 10° the predicted total loads for the body are far above experiment. For wings of rectangular plan form having larger chords relative to the body than the present wing, the negative and positive body loadings were equal at large incidence angles so that the resultant was a couple: zero normal force and large local bending moments.

CONCLUDING REMARKS

Comparisons of the predicted and experimental loadings on wings and wing-body combinations have been presented, from which the following summarizing remarks can be made:

1. On very highly swept delta wings at moderate supersonic Mach numbers, viscosity and separation must be considered, even at low angles of attack, for accurate prediction of load distribution. For wings with less sweepback, but at higher Mach numbers, nonlinear effects of compression and expansion must be considered at all angles of attack.

2. For the wing-body combinations, there were additional nonlinear effects resulting from interference. At large angles of attack the effective body upwash was reduced so that the wing performed essentially as a wing alone. At large angles of wing incidence, unporting of the wing created a body loading which was highly nonlinear.

REFERENCES

1. Kaattari, George E.: Pressure Distributions on Triangular and Rectangular Wings to High Angles of Attack - Mach Numbers 1.45 and 1.97. NACA RM A54D19, 1954.

2. Kaattari, George E.: Pressure Distributions on Triangular and Rectangular Wings to High Angles of Attack - Mach Numbers 2.46 and 3.36. NACA RM A54J12, 1955.

3. Michael, William H., Jr.: Flow Studies on Flat-Plate Delta Wings at Supersonic Speed. NACA TN 3472, 1955.

4. Brown, C. E., and Michael, W. H., Jr.: Effect of Leading-Edge Separation on the Lift of a Delta Wing. Jour. Aero. Sci., vol. 21, no. 10, Oct. 1954, pp. 690-694, 706.

5. Vincenti, Walter G., and Fisher, Newman H., Jr.: Calculation of the Supersonic Pressure Distribution on a Single-Curved Tapered Wing in Regions Uninfluenced by the Root or Tip. NACA TN 3499, 1955.

6. Nielsen, Jack N., Kaattari, George E., and Drake, William C.: Comparison Between Prediction and Experiment for All-Movable Wing and Body Combinations at Supersonic Speeds - Lift, Pitching Moment, and Hinge Moment. NACA RM A52D29, 1952.

7. Allen, H. Julian, and Perkins, Edward W.: A Study of Effects of Viscosity on Flow Over Slender Inclined Bodies of Revolution. NACA Rep. 1048, 1951. (Supersedes NACA TN 2044).

8. Bright, Loren G.: A Flight Investigation at Transonic Speeds of a Model Having a Triangular Wing of Aspect Ratio 4. NACA RM A54L27, 1955.

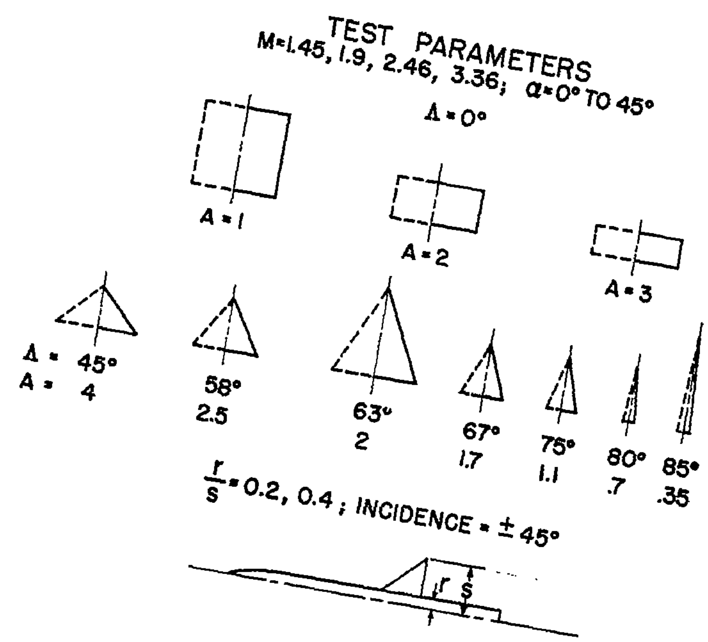

Figure 1

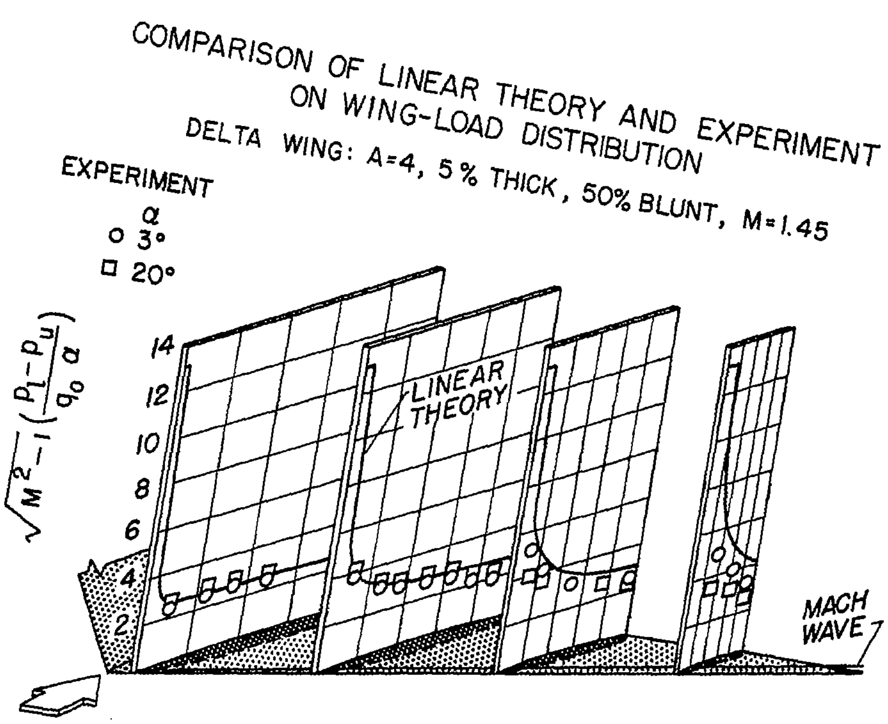

Figure 2

COMPARISON OF THEORY AND EXPERIMENT
FOR PRESSURES

DELTA WING: A=0.35, 1% THICK, 100% BLUNT, M=1.9

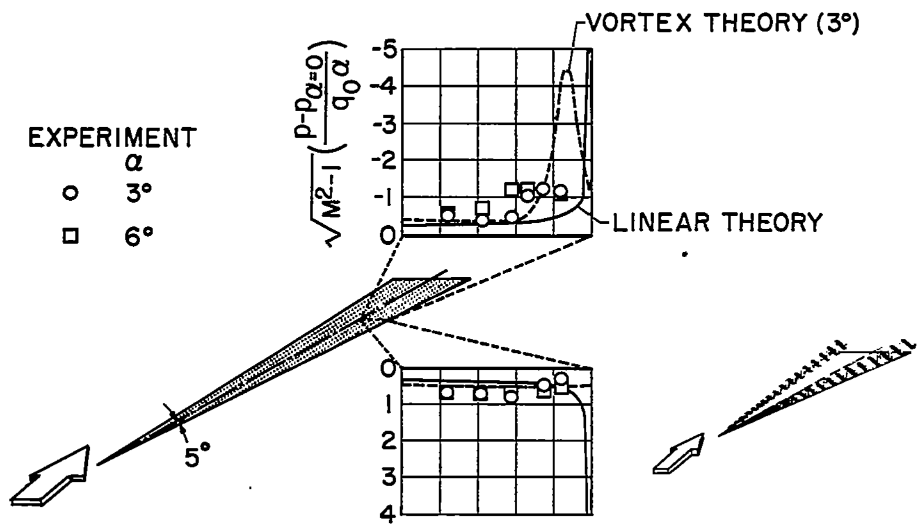

Figure 3

COMPARISON OF LINEAR THEORY AND EXPERIMENT
ON WING-LOAD DISTRIBUTION

DELTA WING: A=4, α=3°, 5% THICK, 50% BLUNT, M=3.36

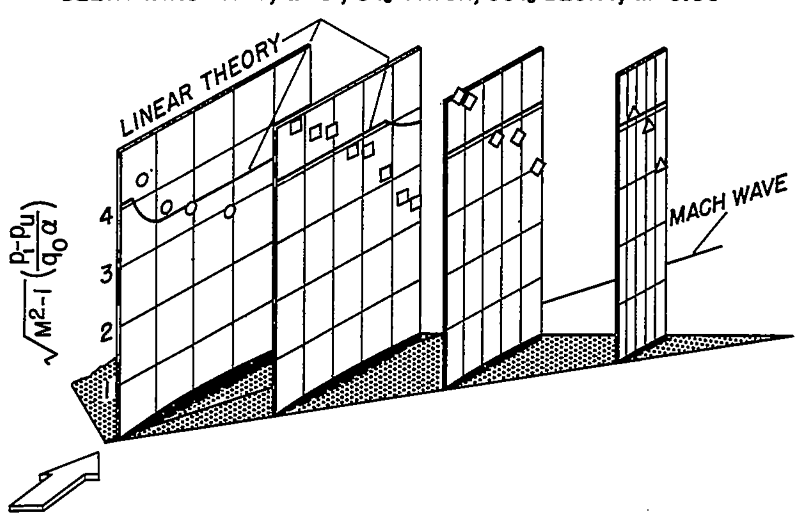

Figure 4

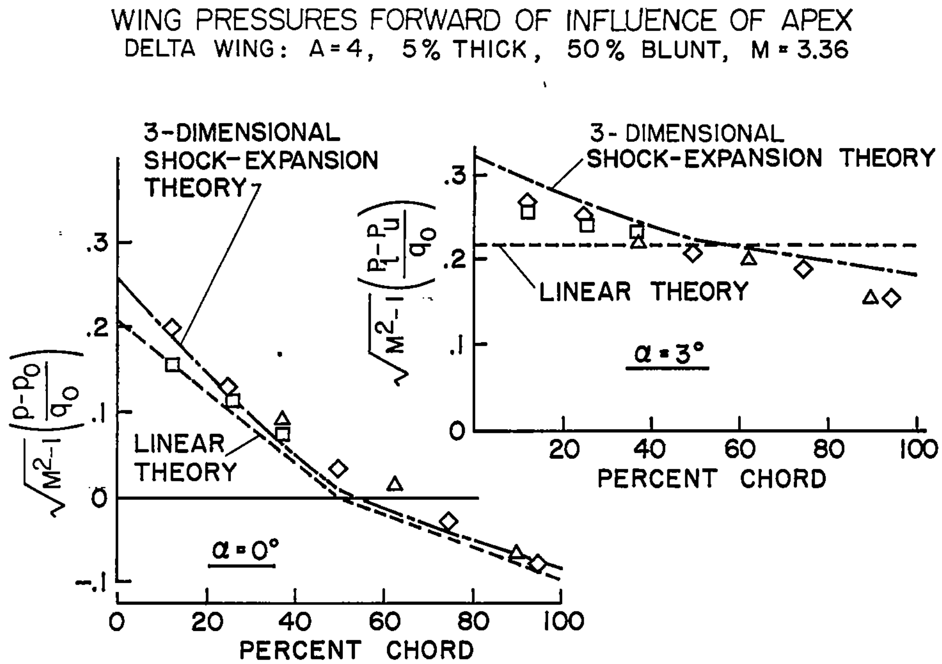

Figure 5

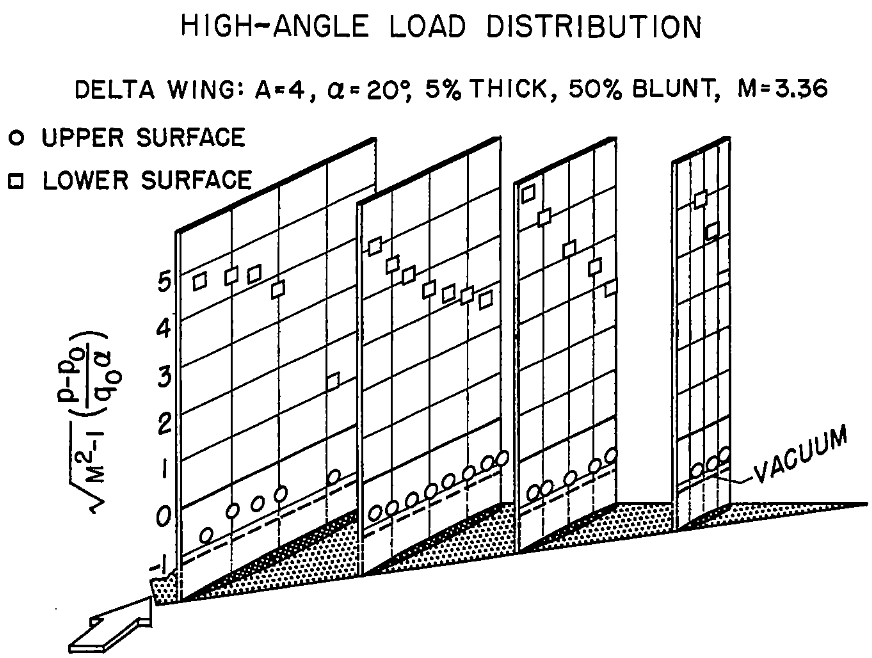

Figure 6

INTERFERENCE ON WING-LOAD DISTRIBUTION
AT ANGLES OF ATTACK
M=3.36

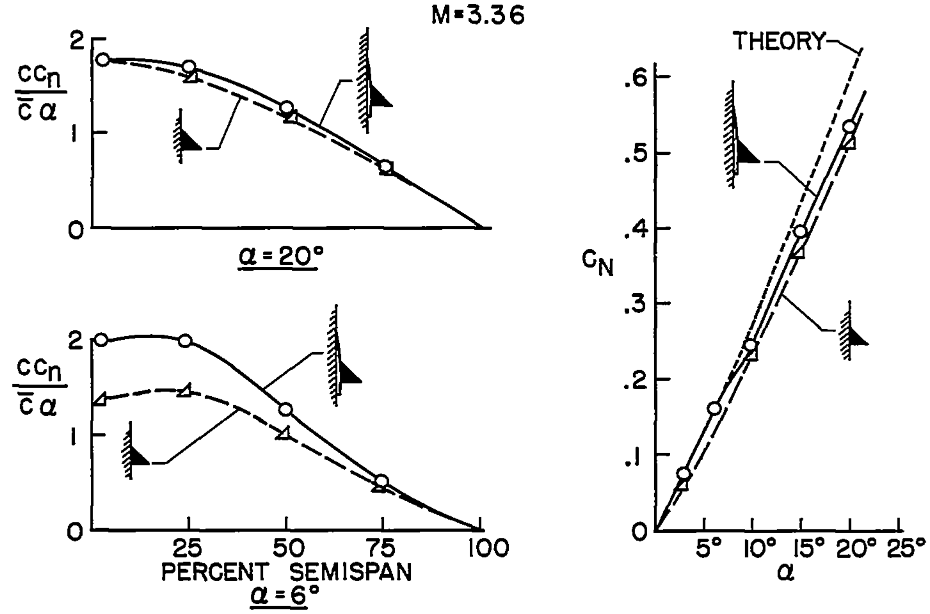

Figure 7

INTERFERENCE ON WING-LOAD DISTRIBUTION
AT ANGLES OF INCIDENCE
M = 3.36

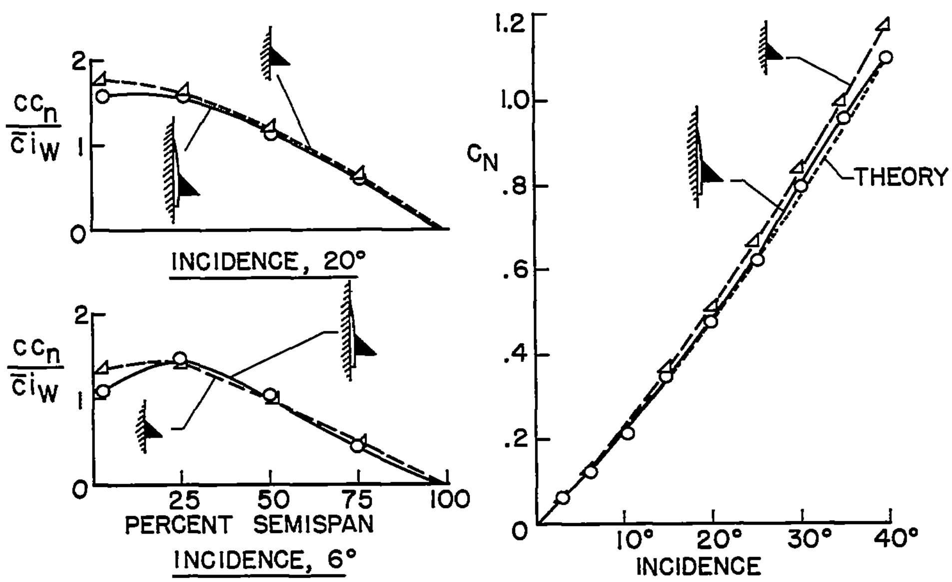

Figure 8

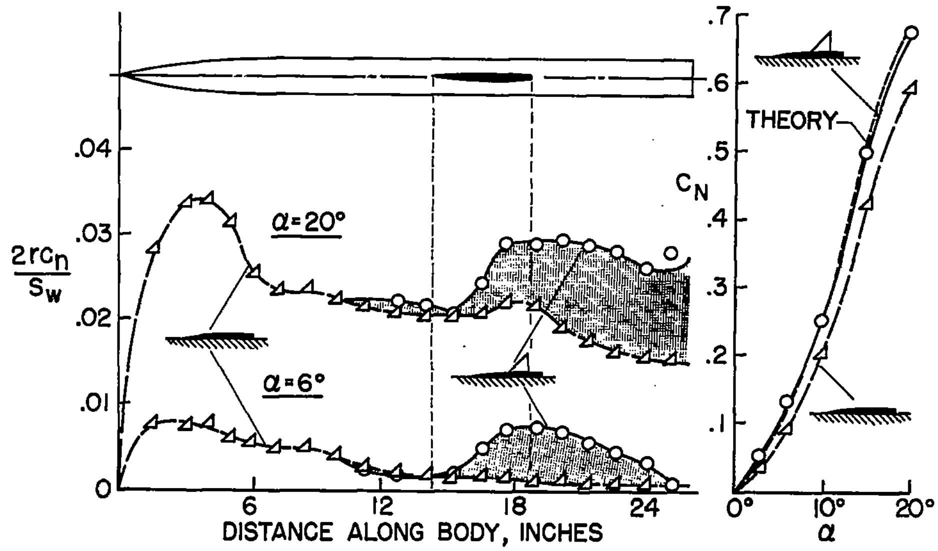

Figure 9

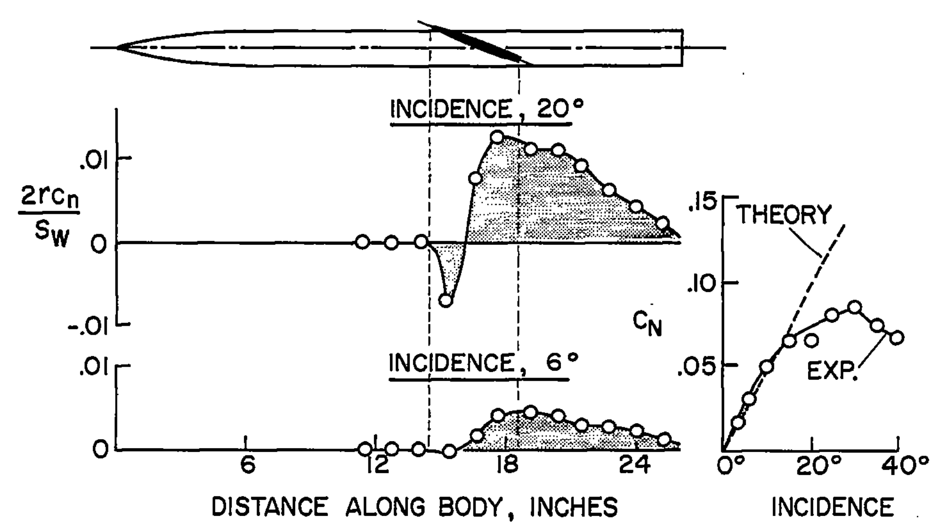

Figure 10

NACA - Langley Field, Va.